# Total flavonoids of Rhizoma Drynariae enhances CD31$^{hi}$Emcn$^{hi}$ vessel formation and subsequent bone regeneration in rat models of distraction osteogenesis by activating PDGF-BB/VEGF/RUNX2/OSX signaling axis

ZHEN SHEN[1*], WEI DONG[1*], ZEHUA CHEN[1*], GUOQIAN CHEN[2], YAN ZHANG[3], ZIGE LI[3], HAIXIONG LIN[3], HUAMEI CHEN[3], MINLING HUANG[3], YING GUO[1] and ZIWEI JIANG[4]

[1]Department of Orthopaedics, Kunming Municipal Hospital of Traditional Chinese Medicine, The Third Affiliated Hospital of Yunnan University of Chinese Medicine, Kunming, Yunnan 650599; [2]The Fifth Clinical Medical College, Guangzhou University of Chinese Medicine, Guangzhou, Guangdong 510405; [3]The First Clinical Medical College, Guangzhou University of Chinese Medicine; [4]Department of Orthopaedics, The First Affiliated Hospital of Guangzhou University of Chinese Medicine, Guangzhou, Guangdong 510407, P.R. China

Received July 21, 2020; Accepted November 19, 2020

DOI: 10.3892/ijmm.2022.5167

**Abstract.** Total flavonoids of *Rhizoma Drynariae* (TFRD), extracted from the kidney-tonifying Traditional Chinese medicine *Rhizoma Drynariae*, can be effective in treating osteoporosis, bone fractures and defects. However, the pharmacological effects of TFRD on the specific vessel subtype CD31$^{hi}$Emcn$^{hi}$ during distraction osteogenesis (DO) remains unclear. The present study aimed to investigate the effects of TFRD on CD31$^{hi}$Emcn$^{hi}$ vessels in a rat model of DO. In the present study, tibial DO models were established using 60 rats with a distraction rate of 0.2 mm per day for 20 days. Co-immunofluorescence staining of CD31 and endomucin (Emcn) was conducted to determine CD31$^{hi}$Emcn$^{hi}$ vessels. Radiographic, angiographic and histological analyses were performed to assess bone and vessel formation. Tube formation, alkaline phosphatase (ALP) and Von Kossa staining assays were performed to test angiogenesis of endothelial precursor cells (EPCs) and osteogenesis of bone marrow-derived mesenchymal stem cells (BMSCs). Additionally, expression levels of platelet-derived growth factor (PDGF)-BB, VEGF, runt-related transcription factor 2 (RUNX2) and Osterix (OSX) were determined by western blotting and reverse transcription-quantitative PCR. The *in vivo* assays demonstrated that TFRD markedly promoted CD31$^{hi}$Emcn$^{hi}$ vessel formation during DO, whereas PDGF-BB neutralizing antibody suppressed vessel formation. Furthermore, the ALP, Von Kossa staining and tube formation assays indicated that TFRD notably elevated the angiogenic capacity of EPCs and osteogenic capacity of BMSCs under stress conditions, which was significantly suppressed by blocking PDGF-BB. The protein and mRNA levels of PDGF-BB, VEGF, RUNX2 and OSX were upregulated by TFRD, but downregulated by blocking PDGF-BB. Thus, TFRD could facilitate CD31$^{hi}$Emcn$^{hi}$ vessel formation and subsequently enhance angiogenic-osteogenic coupling to regenerate bone defects during DO via the PDGF-BB/VEGF/RUNX2/OSX signaling axis, which indicated that CD31$^{hi}$Emcn$^{hi}$ vessels could be a potential novel therapeutic target for DO, and TFRD may represent a promising drug for promoting bone regeneration in DO by increasing CD31$^{hi}$Emcn$^{hi}$ vessels.

*Correspondence to:* Professor Ziwei Jiang, Department of Orthopaedics, The First Affiliated Hospital of Guangzhou University of Chinese Medicine, 16 Jichang Road, Baiyun, Guangzhou, Guangdong 510407, P.R. China
E-mail: jzw1686gzucm@163.com

Professor Ying Guo, Department of Orthopaedics, Kunming Municipal Hospital of Traditional Chinese Medicine, The Third Affiliated Hospital of Yunnan University of Chinese Medicine, 2628 Xiangyuan Road, Chenggong, Kunming, Yunnan 650599, P.R. China
E-mail: gy9501kmszyy@163.com

*Contributed equally

*Key words:* total flavonoids of Rhizoma Drynariae, CD31$^{hi}$Emcn$^{hi}$ vessels, distraction osteogenesis, platelet-derived growth factor-BB, bone regeneration

## Introduction

Distraction osteogenesis (DO) is a well-established surgical procedure to regenerate segmental bone defects in clinical practice (1,2), which consists of three sequential phases: The latency phase after application of external fixation and osteotomy, the distraction phase with the application of regular tensile stress, and the consolidation phase for achieving mineralized bone tissue (3). Although a large number of studies have attempted to investigate the underlying mechanisms of DO-induced bone regeneration from the perspective of microRNAs (4,5), exosomes (6,7) or various biological

materials (8), the limitations of slow callus mineralization and lengthy treatment duration have not been well resolved (9), and even worse, the detailed molecular mechanism of DO in bone repair remains poorly understood (10).

As is commonly known, bone is a highly vascularized tissue (11) and a reduction in vascular supply and limited nutrient availability at the injury site causes impaired bone healing (12), which suggests that angiogenesis is vital to the bone repair process. More importantly, growing evidence (13,14) has demonstrated the close spatial-temporal association and functional codependency that exists between the processes of angiogenesis and osteogenesis during bone repair, which is speculated to be the angiogenic-osteogenic coupling (15). For DO, it is characterized by robust angiogenesis in the distraction phase and subsequent neo-osteogenesis in the later consolidation phase, which indicates the presence of angiogenic-osteogenic coupling during the DO process (16). Previously, a specific vessel subtype called CD31$^{hi}$Emcn$^{hi}$, with high levels of platelet and endothelial cell adhesion molecule-1 and endomucin (Emcn), has been identified in the skeletal system, which has been reported to actively direct bone formation and couple angiogenesis with osteogenesis during bone development and repair (17-19). Although CD31$^{hi}$Emcn$^{hi}$ vessels have been successively found in models of osteoporosis (20), fractures (21) and bone defects (22), it still remains unclear whether CD31$^{hi}$Emcn$^{hi}$ vessels exist in the DO model and whether regular tensile stress could stimulate CD31$^{hi}$Emcn$^{hi}$ vessel formation. Moreover, until the present report, very few studies have been performed to explore drugs that exert positive effects on CD31$^{hi}$Emcn$^{hi}$ vessel formation.

In China, it is well established that the use of Traditional Chinese medicine, such as tonifying kidney herbs, can exert beneficial effects on bone healing and be used as an effective therapeutic strategy in promoting bone formation and repair, when used in combination with other treatments (23). Total flavonoids of *Rhizoma Drynariae* (TFRD), the key ingredient of the commonly known kidney-tonifying Traditional Chinese medicine *Rhizoma Drynariae*, has been demonstrated to have pharmacological effects on the skeleton system. These actions include upregulating the expression levels of bone morphogenetic protein 2 and runt-related transcription factor 2 (RUNX2) (24), and promoting osteoblast proliferation and differentiation (25). As reported previously, the active compounds in TFRD are naringin and neoeriocitrin (26). At present, TFRD has been developed into a Chinese patent medicine called Qianggu Capsule (drug approval no. Z20030007, Beijing Qihuang Pharmaceutical Co., Ltd.). We previously reported that TFRD can accelerate bone formation and remodeling in the distracted gap (27). Moreover, TFRD was also found to have the potential to promote vascularization during DO (27). However, whether TFRD influences CD31$^{hi}$Emcn$^{hi}$ vessels and the underlying mechanism during DO remains unknown.

Given that CD31$^{hi}$Emcn$^{hi}$ vessels play a critical role in coupling angiogenesis and osteogenesis during bone development and repair, it was hypothesized in the present study that CD31$^{hi}$Emcn$^{hi}$ vessels exist in the DO model and TFRD treatment contributes to bone regeneration by stimulating the formation of CD31$^{hi}$Emcn$^{hi}$ vessels during DO. The aim of the present study was to observe whether CD31$^{hi}$Emcn$^{hi}$ vessels exist in the DO model and whether TFRD could promote CD31$^{hi}$Emcn$^{hi}$ vessel formation, and further investigate the potential mechanism of CD31$^{hi}$Emcn$^{hi}$ vessel-mediated bone repair during DO.

## Materials and methods

*Identification for active compounds of TFRD*. The active compounds of TFRD were identified by liquid chromatography-mass spectrometry (LC-MS) using high- performance liquid chromatography (HPLC; TSQ Quantum™; Thermo Fisher Scientific, Inc.) and MS (UltiMate™ 3000 RS; Thermo Fisher Scientific, Inc.). Briefly, solution (10 $\mu$l) was subjected to HPLC and analyzed with a UV detector (SPD-M20A; Shimadzu Corporation) at 283 nm. The mobile phase was composed of (A) methanol and (B) 0.1% acetic acid water, with a gradient elution as follows: 0~14 min, 30-35% A; 14~22 min, 35-50% A; 22~26 min, 50-35% A; 26~35 min, and 35-35% A. The flow rate of the mobile phase was 1.0 ml/min. The chromatographic column was a C18 (4.6x250 mm, ID, 5 $\mu$m; Merck KGaA). The MS identification conditions were as follows: The ion source was ESI, the atomization pressure was 35 psi, the dry gas flow rate was 11 ml/min, the mass range of mass spectrometry was 100~1,000 amu, and the ion mode was negative. The reference solutions were prepared directly in methanol: naringin (CAS no. 10236-47-2; batch, 23,616; Aladdin Bio-Tech Group) and neoeriocitrin (CAS no. 13241-32-2; batch, ASB-00005190-010; ChromaDex Standards). Working standard solutions containing the two compounds were prepared and diluted with methanol to the appropriate concentrations for the establishment of calibration curves. The TFRD samples were also dissolved in methanol and prepared as working solutions. The reference solutions and working solutions were all prepared in dark brown calibrated flasks and stored at 4˚C. The chromatogram collection and integration of naringin were processed by Xcalibur™ 3.0 software (Thermo Fisher Scientific, Inc.). The peak area of naringin or neoeriocitrin was taken as the ordinate and the concentration of naringin or neoeriocitrin as the abscissa. The standard curve line was obtained by linear regression analysis with Equal as the weighted coefficient.

*Animal surgical procedure and experimental design*. A total of 60 adult male Sprague-Dawley (SD) rats (SIPPR-BK Experimental Animal, Ltd.) age, 20 weeks; weight, 380-420 g) were kept in specific pathogen-free housing in the laboratory with standard conditions at 24˚C in 50-70% humidity under 12/12 h light/dark cycle. SD rats were subjected to the tibial DO model and then randomly divided into four groups (n=15 per group): i) TFRD group; ii) TFRD+platelet-derived growth factor (PDGF)-BB-neutralizing antibody (Ab) group; iii) PDGF-BB-Ab group; and iv) control group. The DO model was established as described previously (28). In brief, as shown in Fig. 1, after rats were anesthetized with an intraperitoneal injection of pentobarbital (3 mg/100 g; Sigma-Aldrich; Merck KGaA), a longitudinal incision was made in the skin distal to the right tibia crest and the bone was exposed. Meanwhile, surgical scissors were used to cut the fibula. Then, a custom-made circle external device was assembled and fixed to the tibia by four 27-gauge stainless steel needles (Zhangjiagang Baokang

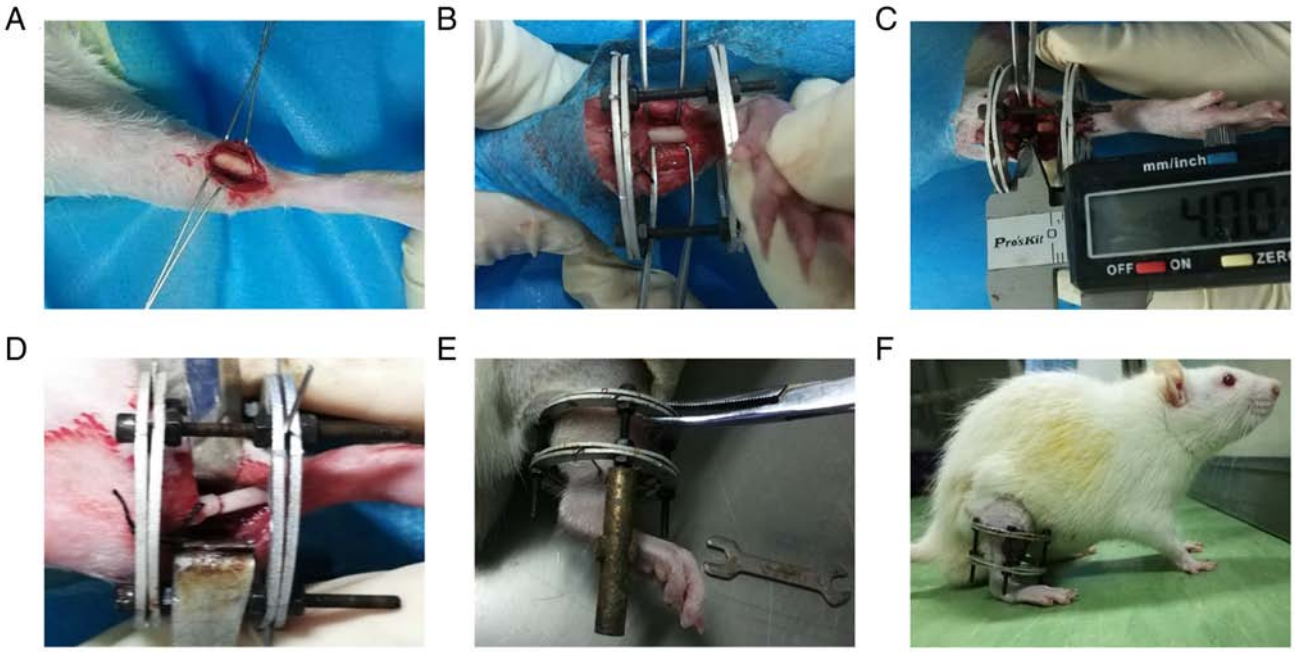


Figure 1. Flowchart of surgical procedures of distraction osteogenesis model using an external fixator. (A) Tibia exposure. (B) Fixation using the external fixator. (C) Osteotomy. (D) Shortening and aligning osteotomy. (E) Distraction procedure. (F) Consolidation stage.

Medical Equipment Co., Ltd.). After stabilization, transverse corticotomies using a Gigli saw (Zhangjiagang Baokang Medical Equipment Co., Ltd.) were performed to create a 4-mm long diaphyseal defect on the tibia. Thereafter, the two osteotomy surfaces were in close contact and aligned. Finally, the wound was irrigated with sterile saline and then closed layer by layer. Following surgery, rats were given access to food and water *ad libitum*. Amoxicillin (1.5 mg/100 g weight) and buprenorphine (1.0 mg/kg weight) were administered intraperitoneally for 3 days after surgery. After a 7-day latency period, the distraction procedure was initiated at a rate of 0.1 mm/12 h until the length of the shortened tibia induced by osteotomy was restored. Then, the consolidation stage lasted for 4 weeks. According to a previous study (29), rats were administered with TFRD orally at a dose of 75 mg/kg body weight/day, and then rats in the TFRD group were injected intraperitoneally with an equal amount of PBS, whereas rats in the PDGF-BB-Ab group were injected intraperitoneally with 20 g/ml PDGF-BB-Ab (Abcam) and orally fed with an equal amount of PBS. The TFRD+PDGF-BB-Ab group received an intraperitoneal injection of 20 g/ml PDGF-BB-Ab combined with an oral administration of TFRD at a dose of 75 mg/kg body weight/day. The control group was subjected to intraperitoneal and oral administration of equal amounts of PBS. From day 1 post-surgery, TFRD was administrated once a day and PDGF-BB-Ab was injected once a week until termination of the study. In the present study, the rats were intraperitoneally injected with pentobarbital (10 mg/100 g) for euthanasia. In addition, complete cardiac and respiratory arrest, and pupil dilation were observed to indicate that the rat had been successfully euthanized. All animal care and experimental procedures were approved by the Institutional Animal Ethics Committee of the First Affiliated Hospital of Guangzhou University of Traditional Chinese Medicine (approval no. TCMF1- 2018002; Guangzhou, China).

*Micro-CT analysis*. According to a previous study (30), the distracted tibia specimens (n=3 per group) were harvested and scanned with micro-CT (SkyScan 1076; Bruker Corporation) at a resolution of 20 $\mu$m (70 kV and 130 $\mu$A radiation source with 0.5 mm aluminum filter), after consolidation for 4 weeks. Bone tissue volume/total tissue volume (BV/TV) inside the distracted gaps were analyzed using CTAN software (v1.9; Bruker Corporation). The test was repeated with three specimens.

*Angiography analysis*. For angiography analysis, three rats per group were anesthetized and perfused with Microfil (MICROFIL® MV-122; Flow Tech, Inc.) after consolidation for 4 weeks, as described previously (7). Briefly, the rib cage was opened after anesthetization, the descending aorta was clamped, and the inferior vena cava was incised. Subsequently, the vasculature was flushed with 0.9% normal saline containing heparin sodium (100 U/ml) and 20 ml Microfil were perfused into the left ventricle with an angiocatheter. Subsequently, the rats were stored at 4˚C overnight to ensure polymerization of the contrast agent, after which the tibias were dissected, fixed in 4% paraformaldehyde for 48 h at room temperature, decalcified in 10% EDTA for 4 weeks and then imaged by micro-CT.

*Histological and immunofluorescent analyses*. At 4 weeks post-distraction, tibia specimens (n=3 per group) were taken, decalcified in 10% EDTA for 4 weeks, dehydrated through increasing concentrations of ethanol, and then embedded in paraffin. Thereafter, the specimens were cut into 5 $\mu$m thick longitudinally oriented sections, and immunostaining blocking buffer (cat. no. P0102; Beyotime Institute of Biotechnology) was used to block sections overnight at 4˚C. Some sections were processed for hematoxylin and eosin (H&E, stained at room temperature for 5 and 2 min, respectively), Masson's

trichrome (Weigert staining for 5 min, Masson blue for 5 min and Ponceau S staining for 7 min at room temperature) and Safranin O staining (Fast Green staining for 7 min and Safranin O for 20 sec at room temperature). Other sections were used for immunofluorescent staining. For determination of CD31$^{hi}$Emcn$^{hi}$ vessels, some sections were subjected to double immunofluorescence staining for CD31 (1:50; cat. no. sc-71873; Santa Cruz Biotechnology, Inc.) and Emcn (1:50; cat. no. sc-65495; Santa Cruz Biotechnology, Inc.). Briefly, bone sections were stained with individual primary antibodies overnight at 4˚C, followed by staining with secondary antibodies (1:50; cat. no. A0208, Beyotime Institute of Biotechnology) conjugated with fluorescence at room temperature for 1 h. Nuclei were stained with DAPI (0.5 $\mu$g/ml, 5 min at room temperature). Meanwhile, some sections were incubated with anti-RUNX2 (1:100; cat. no. ab76956; Abcam), anti-Osterix (OSX; 1:100; cat. no. ab22552; Abcam), anti-CD31 (1:100; cat. no. sc-71873; Santa Cruz Biotechnology, Inc.) and anti-PDGF-BB (1;100; cat. no. ab21234; Abcam) primary antibodies at 4˚C for 24 h, and then stained with secondary antibodies (1:50; cat. no. A0208; Beyotime Institute of Biotechnology) conjugated with fluorescence at room temperature for 1 h. Images were acquired with a Leica DMI6000B fluorescence microscope (Leica Microsystems GmbH). The number of positively stained cells or area in five random fields of the distracted zone in three random sections from each specimen were analyzed and all tests were repeated with three specimens.

*Western blotting*. Three rats in each group were randomly selected for western blotting. In brief, after bone samples were lysed using RIPA lysis and Extraction buffer (Nanjing KeyGen Biotech Co., Ltd.), a BCA protein assay kit (cat. no. ab102536; Abcam) was used to measure the protein concentrations, according to the manufacturer's instructions (Varioskan Flash; Thermo Fisher Scientific, Inc.). Each protein sample (40 g) was subjected to SDS-PAGE on a 10% gel, and then electroblotted onto a polyvinylidene difluoride membrane (0.45 mm; EMD Millipore). Subsequently, the membranes were blocked with 5% (w/v) non-fat dry milk in TBS with 0.05% Tween-20 (Beyotime Institute of Biotechnology) at room temperature for 45 min, followed by incubation with primary anti-PDGF-BB (1:500; cat. no. ab21234; Abcam), anti-VEGF (1:500; cat. no. sc-7269; Santa Cruz Biotechnology, Inc.), anti-RUNX2 (1:1,000; cat. no. ab23981; Abcam), anti-OSX (1:1,000; cat. no. ab22552; Abcam), anti-phosphorylated (p)-AKT (1:1,000; cat. no. ab81283; Abcam), p-PDGFR-β (1:2,000; cat. no. AF3132; Affinity Biosciences), PDGFR-β (1:2,000; cat. no. AF6133; Affinity Biosciences), AKT (1:1,000; cat. no. 4691; Cell Signaling Technology, Inc.), ERK (1:2,000; cat. no. AF0155; Affinity Biosciences) and anti-p-ERK1/2 (1:1,000; cat. no. ab214362; Abcam) antibodies at 4˚C overnight. Then, the membranes were incubated with the horseradish peroxidase-conjugated secondary antibodies (1:5,000; cat. no. ab205718; Abcam) for 1 h at room temperature. BeyoECL Plus reagent (cat. no. P0018S; Beyotime Institute of Biotechnology) was used for visualization. The protein levels were normalized against β-actin (1:1,000; cat. no. 4970; Cell Signaling Technology, Inc.). Representative bands were selected from the three independent experiments. Densitometric analysis was performed using ImageJ software (v1.8.0.112; National Institutes of Health).

*Reverse transcription-quantitative (RT-q)PCR*. The newly-formed tissues inside the distracted gaps of three rats per group were carefully and quickly collected at 4 weeks post-distraction. All procedures were performed at 4˚C. The total cellular RNA of the tissues was extracted using TRIzol® reagent (Invitrogen; Thermo Fisher Scientific, Inc.), according to the manufacturer's instructions. RNA samples collected from the distracted tibias were examined by measuring the ratio of the optical density at 260 and 280 nm (OD 260/280). Samples with a ratio of 2.0 were used for reverse transcription. cDNA was synthesized using 1 $\mu$g RNA and a RevertAid First Strand cDNA Synthesis kit (Takara Biotechnology Co., Ltd.). RT-qPCR was performed in triplicate using a PrimeScript™ RT reagent kit with gDNA Eraser (cat. no. RR047A; Takara Biotechnology Co., Ltd.) followed by a TB Green® Premix EX Taq™ II kit (cat. no. RR820A; Takara Biotechnology Co., Ltd.). The thermocycling conditions were as follows: Pre-denaturation at 95˚C for 30 sec, followed by 45 cycles of 95˚C for 10 sec, 57˚C, 58˚C or 60˚C for 15 sec, and 72˚C for 10 sec. Cycle quantification values for the samples were normalized to that of β-actin and the relative expression was calculated using the $2^{-\Delta\Delta Cq}$ method (31). The primer sequences used are listed in Table SI.

*Cell culture*. Endothelial precursor cells (EPCs) and bone marrow-derived mesenchymal stem cells (BMSCs) were cultured following previous techniques (32), with minor modifications. Briefly, the bone marrow cavities of femurs and tibias were washed at 4˚C in 0.01 M PBS. Mononuclear cells were collected from marrow suspension and then cultured with EGM-2 MV medium (Lonza Group, Ltd.) for EPC culture, or cultured in Mesenchymal Stem Cell Growth Medium (Lonza Group, Ltd.) for BMSC culture. After 24 h of culture, the attached cells were plated into a 50 ml glass flask coated with fibronectin (Sigma-Aldrich; Merck KGaA) at a density of $1.0x10^6$ per liter and the medium was changed every 3 days. Cells at passage 3 were used for subsequent experiments.

*Establishment of stress conditions*. As described previously (33), the stress conditions were established using the STREX cell stretching system (ST-160; Amuza, Inc.) to apply regular tensile stress to cells in a single, parallel direction at an approximate ratio of 10%.

*Cell migration assay*. The migratory ability of EPCs was evaluated via a Transwell migration assay (Costar; Corning, Inc.). Third passage EPCs at a density of $1x10^4$/well were loaded into the upper chamber of 24-well, 8-$\mu$m pore-size Transwell plates (Corning, Inc.) with a polycarbonate membrane that contained serum-free endothelial growth medium(Lonza Group, Ltd.). Subsequently, medium containing TFRD (100 $\mu$g/ml) or PDGF-BB-Ab (20 $\mu$g/ml) diluted with low-glucose DMEM (Gibco; Thermo Fisher Scientific, Inc.) supplemented with 10% FBS was added to the lower chambers. After co-incubation for 24 h at 37˚C under 5% $CO_2$, non-migrated cells that remained in the upper chambers were removed by wiping the top of the insert membranes with cotton swabs, while the migrated cells

that passed through the membrane pores were stained with 0.5% crystal violet for 20 min at 37˚C and counted under an optical microscope (Leica Microsystems GmbH). Five random fields of view were used to count the number of migrated cells, this assay was performed in triplicate.

*Alkaline phosphatase (ALP) staining and activity assay.* After 7 days of osteogenic induction, ALP staining was performed to assess the osteogenic differentiation potential of BMSCs. Briefly, BMSCs were fixed for 20 min at 37˚C in 4% paraformaldehyde, washed three times with distilled water, and subsequently stained with the Alkaline Phosphatase Assay kit (Beyotime Institute of Biotechnology) at 37˚C for 30 min. For ALP activity, BMSCs were lysed with lysis buffer (20 mM pH 7.5 Tris HCl, 150 mM NaCl and 1% Triton X-100) in 96-well plates, and the substrates and p-nitrophenol were added. ALP activity was analyzed by determining the absorbance at 405/650 nm.

*Von Kossa staining.* After 21 days of osteogenic induction, calcium mineral deposition was measured through Von Kossa staining. Briefly, BMSCs were fixed as described above and washed for Von Kossa staining. Following incubation in 5% silver nitrate for 10 min at 37˚C, BMSCs were exposed to light for 30 min and washed in 5% sodium thiosulphate for 5 min to remove non-specific staining. Cells were observed under an inverted microscope (Leica Microsystems GmbH).

*Matrigel tube formation assay.* Matrigel Growth Factor Reduced Basement Membrane Matrix (cat. no. 356230; Corning, Inc.) was used to assess the tube formation of EPCs, which was thawed on ice. Then, each well was coated with 100 $\mu$l Matrigel at 37˚C for 30 min, according to the manufacturer's instructions. EPCs ($6x10^4$ cells per well) were seeded onto Matrigel-coated 24-well plates and cultured with or without TFRD (100 $\mu$g/ml) at 37˚C and 5% $CO_2$ for 6 h, some cells were pretreated with PDGF-BB-Ab (20 $\mu$g/ml) for 1 h before TFRD treatment. After incubation for 6 h, cells were observed with an inverted microscope (Leica Microsystems GmbH). Total tube length in five randomly chosen fields were quantified using ImageJ v1.8.0 software (National Institutes of Health).

*Statistical analysis.* All data are presented as the mean ± standard deviation. SPSS 19.0 software (IBM Corp.) was used to analyze experimental data. Differences among groups were assessed by one-way analysis of variance (ANOVA), followed by a Tukey's post hoc test. $P<0.05$ was considered to indicate a statistically significant difference.

## Results

*Active compounds of TFRD.* The LC-MS results demonstrated that the active ingredients of TFRD included naringin and neoeriocitrin. The chemical structures and formulas of naringin and neoeriocitrin are presented in Fig. 2A and B. Based on the results in Fig. 2C and D, the peak at the time point of '1.91' and '1.97' in the total ion chromatogram of TFRD sample refers to neoeriocitrin and naringin, respectively. As shown in the standard curve lines of Figs. S1A-C and S2A-C, the concentrations of naringin and neoeriocitrin in 1 $\mu$g TFRD sample were 173.082 and 131.833 ng/ml, respectively.

*Administration of TFRD increases the abundance of $CD31^{hi}Emcn^{hi}$ vessels during DO in rats.* As shown in Fig. 3A-C and Table SII, the CD31 and Emcn immunofluorescent staining results demonstrated the presence of $CD31^{hi}Emcn^{hi}$ vessels during the process of DO and a higher proportion of $CD31^{hi}Emcn^{hi}$ vessels were observed in the TFRD group compared with the control group at 4 weeks post-distraction. Compared with the control group, a significant decline in the abundance of $CD31^{hi}Emcn^{hi}$ vessels was observed in the PDGF-BB-Ab group. Of note, this decline was significantly attenuated by the addition of TFRD, as demonstrated by the significantly higher abundance of $CD31^{hi}Emcn^{hi}$ vessels observed in the TFRD+PDGF-BB-Ab group. Thus, these results indicated that TFRD can promote $CD31^{hi}Emcn^{hi}$ vessel generation during DO, whereas PDGF-BB-Ab suppresses the formation of $CD31^{hi}Emcn^{hi}$ vessels.

*TFRD facilitates angiogenesis and osteogenesis during DO in rats.* As presented in Fig. 4A and B and Table SIII, TFRD treatment resulted in a significant increase in angiogenesis compared with the control and PDGF-BB-Ab groups. Similar to the manifestation of angiogenesis, the micro-CT images indicated increased newly-formed callus within the distracted gap in the TFRD group than in the other three groups. For the TFRD group, complete bony union inside the distracted gap was achieved, while partial bony union or no obvious radiographical defect bridging occurred in the other three groups (Fig. 4C). The BV/TV of the TFRD group was significantly higher compared with the control and PDGF-BB-Ab groups (Fig. 4D and Table SIII). Meanwhile, histological analyses further confirmed the aforementioned findings. The TFRD group showed complete defect healing and had the most improved bone connection and integration, with both newly-formed bone tissue bridging the defects and bone marrow filling the gap, while moderate immature new bone formation with osteoid matrix appeared inside the distracted gaps in the TFRD+PDGF-BB-Ab group and only chondroid matrix accompanied with fibrous connective tissues filled the gaps in the PDGF-BB-Ab and control groups (Fig. 4E). Therefore, combined with the results in Fig. 3, groups with higher abundance of $CD31^{hi}Emcn^{hi}$ vessels showed increased bone and vessel formation in the distracted gaps, whereas groups with lower abundance of $CD31^{hi}Emcn^{hi}$ vessels showed a decreased amount of bone and vessel formation.

*TFRD enhances the angiogenic capacity of EPCs and the osteogenic capacity of BMSCs under stress conditions.* As revealed by the tube formation assay, the total tube length was significantly higher following TFRD treatment, compared with the control and PDGF-BB-Ab groups (Fig. 5A and C and Table SIV). In addition, the cell migration assay suggested that TFRD significantly enhanced the number of migrated cells compared with the control and PDGF-BB-Ab groups under stress conditions (Fig. 5B and D and Table SIV). Meanwhile, the *in vitro* ALP (Fig. 5E) and Von Kossa staining (Fig. 5G) assays showed increased staining and calcium deposits in the TFRD-treated groups compared with the control and

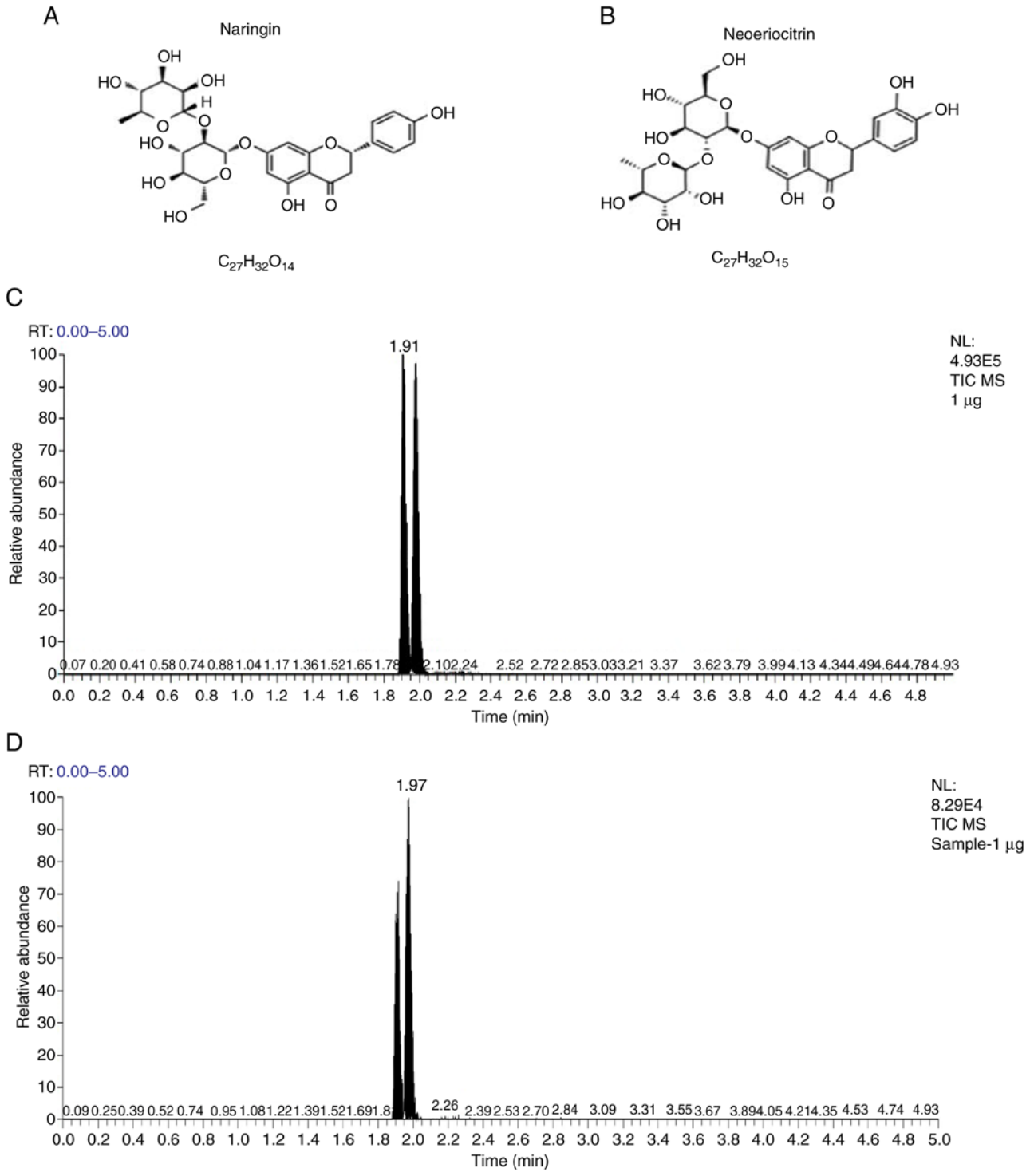


Figure 2. Identification of the active compounds in TFRD by liquid chromatograph-mass spectrometry. The chemical structures and formulas of (A) naringin and (B) neoeriocitrin. (C) TIC of the reference substances (1 $\mu$g/ml). (D) TIC of the TFRD sample. The peak at the time point of '1.91' is neoeriocitrin and the peak at the time point of '1.97' is naringin. TFRD, total flavonoids of *Rhizoma drynariae*; TIC, total ion chromatogram.

PDGF-BB-Ab groups under stress conditions. Furthermore, quantitative results of ALP activity and Von Kossa staining demonstrated that TFRD treatment significantly increased ALP activity and calcium mineral deposition compared with the control and PDGF-BB-Ab groups (Fig. 5F and H and Table SV). However, the aforementioned effects were blocked by PDGF-BB-Ab. Thus, these results indicated that TFRD significantly elevated the osteogenic capacity of BMSCs and angiogenic capacity of EPCs under stress conditions, whereas PDGF-BB-Ab weakened these effects.

*TFRD promotes CD31$^{hi}$Emcn$^{hi}$ vessel formation in angiogenic-osteogenic coupling during DO via the PDGF-BB/platelet-derived growth factor receptor (PDGFR)-β pathway.* As shown in Fig. 3, the group treated with PDGF-BB-Ab showed the lowest abundance of

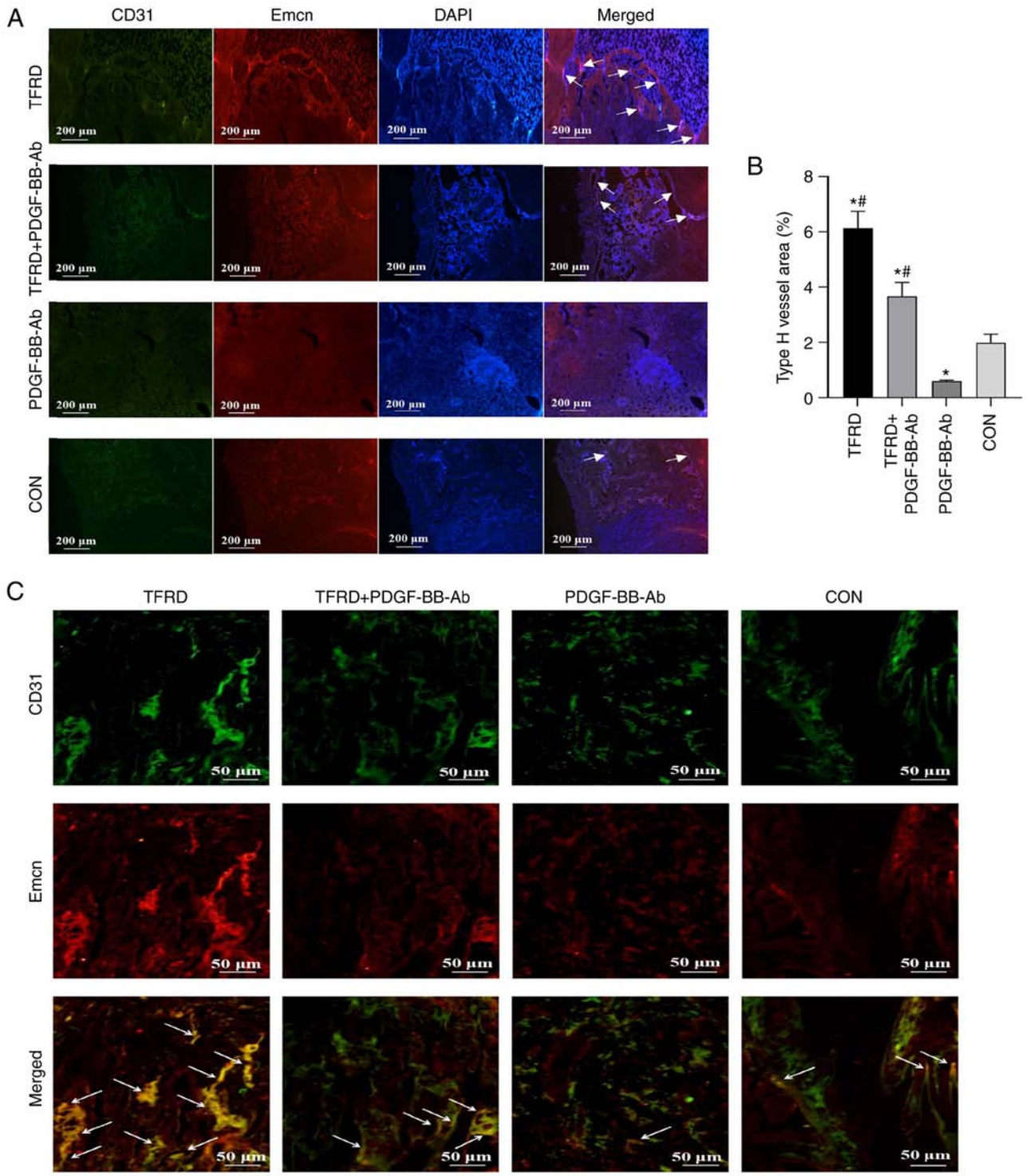


Figure 3. TFRD promotes the formation of CD31$^{hi}$Emcn$^{hi}$ vessels during the distraction osteogenesis process. (A) Representative immunostaining images of CD31 (green), Emcn (red) and Nuclei (blue, stained with DAPI) inside the distracted regions of four groups at 4 weeks post-distraction. The white arrows represent the CD31$^{hi}$Emcn$^{hi}$ vessels. Scale bar, 200 $\mu$m. (B) Quantification of CD31$^{hi}$Emcn$^{hi}$ (light pink) vessel area within the distracted gaps at 4 weeks post-distraction. (C) Representative images of CD31$^{hi}$Emcn$^{hi}$ vessels inside the distracted gaps at a higher magnification. Scale bar, 50 $\mu$m. Data represent the mean ± SD. n=3 for each group from three independent experiments. $^{*}$P<0.05 vs. control group; $^{\#}$P<0.05 vs. PDGF-BB-Ab group. TFRD, total flavonoids of *Rhizoma drynariae*; PDGF, platelet-derived growth factor; Emcn, endomucin.

CD31$^{hi}$Emcn$^{hi}$ vessels. More importantly, upon downregulation of CD31$^{hi}$Emcn$^{hi}$ vessel expression, both osteogenesis and angiogenesis inside the distracted gaps during DO were suppressed, as revealed by micro-CT, angiography and histological analyses (Fig. 4). Furthermore, the immunofluorescent assays further verified the radiographical and histological analyses, which demonstrated that the expression levels of osteogenesis-related markers, including RUNX2 and OSX, as well as the expression levels of angiogenesis-related markers, including CD31 and PDGF-BB, were significantly lower in the PDGF-BB-Ab group compared with the control group, which was significantly reversed by TFRD treatment

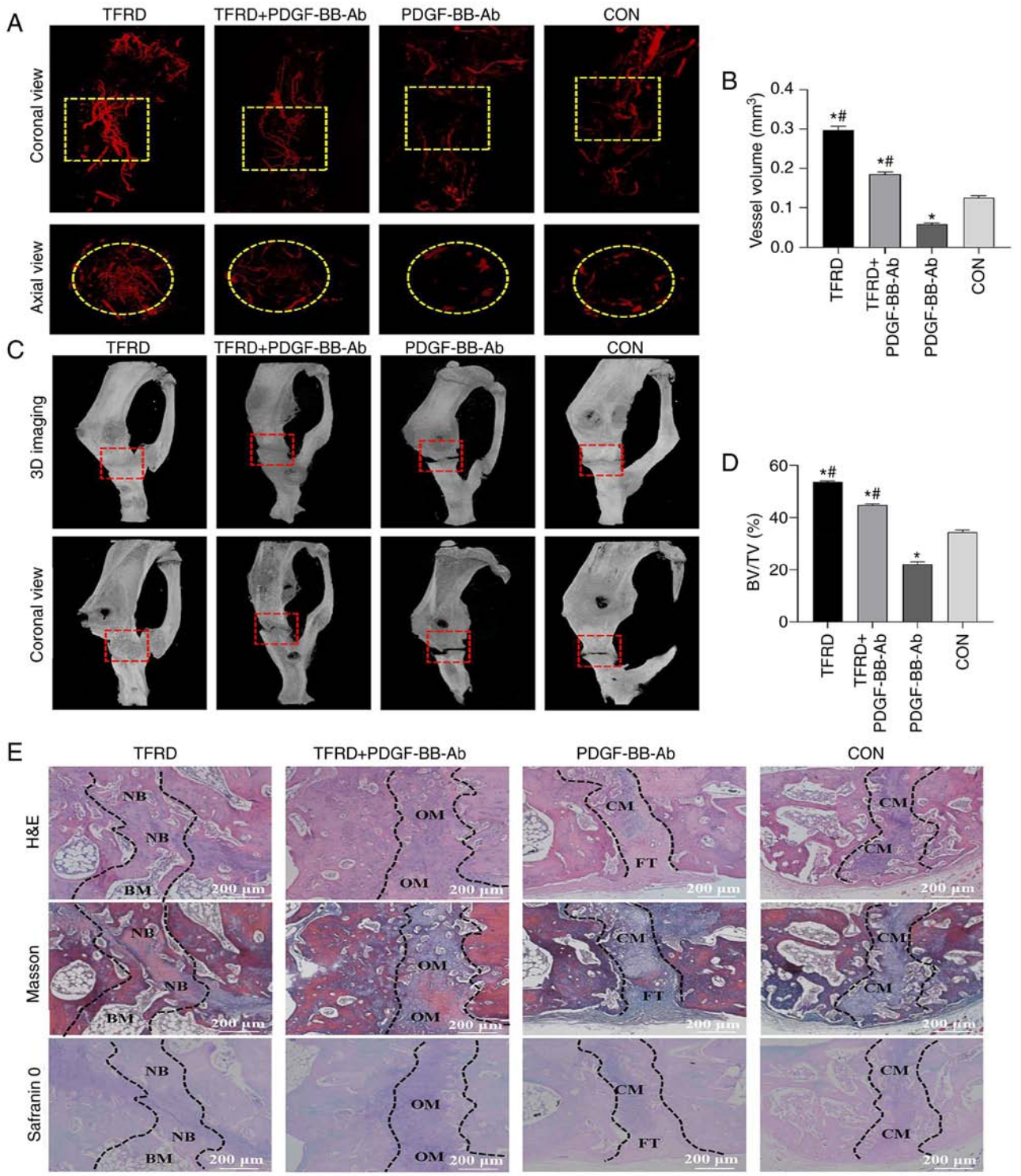


Figure 4. TFRD facilitates angiogenesis and osteogenesis the distraction osteogenesis process in rats. (A) Representative angiographic images and (B) quantification of the vessel volume inside the distracted gaps of four groups at 4 weeks post-distraction in both coronal (top panel) and axial (lower panel) views. Yellow dotted boxes indicate the region of interest. (C) Representative micro-CT images and (D) quantification of bone regeneration within the distracted gaps at 4 weeks post-distraction. Red dotted boxes indicate the region of interest, representing the distracted gaps. (E) Representative histological images including H&E, Masson's trichrome and Safranin O staining of the newly-formed tissues within the distracted gaps 4 weeks post-distraction. Scale bar, 200 $\mu$m. The regions between the two black dotted lines represent the distracted zones. Data represent the mean ± SD. $^{*}$P<0.05 vs. control group; $^{\#}$P<0.05 vs. PDGF-BB-Ab group. TFRD, total flavonoids of *Rhizoma drynariae*; PDGF, platelet-derived growth factor; BV/TV, bone tissue volume/total tissue volume; NB, newly-formed bone; BM, bone marrow; OM, osteoid matrix; CM, chondroid matrix; FT, fibrous tissue; H&E, hematoxylin and eosin; 3D, three-dimensional.

(Fig. 6A and B and Table SVI). Additionally, the angiogenic capacity of EPCs and osteogenic capacity of BMSCs under stress conditions were also weakened in the PDGF-BB-Ab group (Fig. 5). Once PDGF-BB-Ab was administrated to rats during DO or added to the culture media under stress conditions, the TFRD-induced positive effects on osteogenesis and osteogenesis were also reduced. As presented in Fig. 6C-E and Tables SVII and SVIII, the results of western blotting

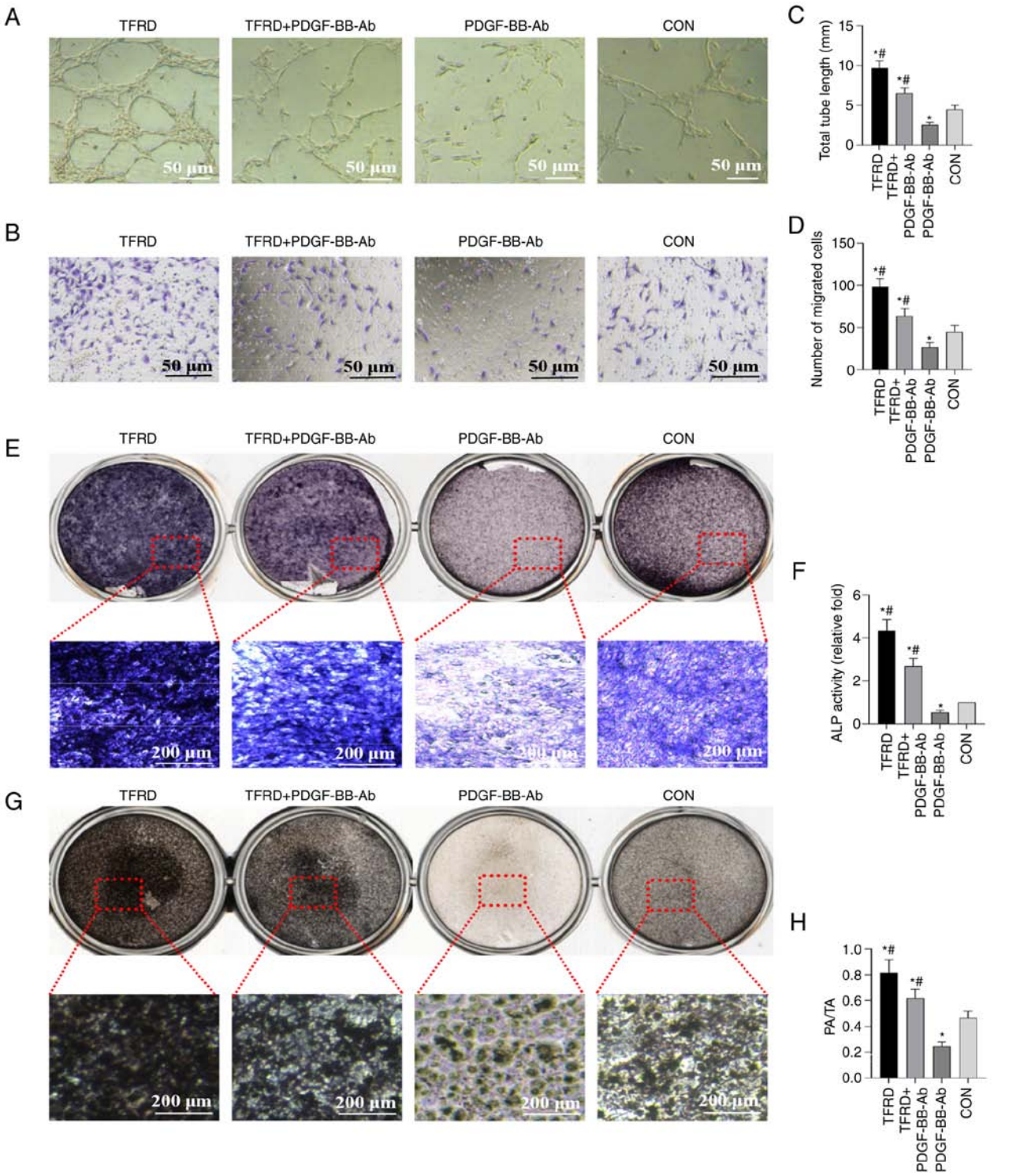


Figure 5. TFRD enhances the angiogenic capacity of EPCs and the osteogenic capacity of bone marrow-derived mesenchymal stem cells under stress conditions. Representative photomicrographs of (A) tube formation and (B) cell migration of EPCs stimulated with 100 $\mu$g/ml TFRD or 20 $\mu$g/ml PDGF-BB-Ab for 6 h under stress conditions. Quantification of (C) tube formation and (D) cell migration. Scale bar, 50 $\mu$m. (E) Representative images of ALP staining and (F) quantitative determination of ALP activity following culture for 7 days under stress conditions. (G) Representative images of Von Kossa staining and (H) quantitation of calcium mineral deposition following culture for 21 days under stress conditions. Scale bar, 200 $\mu$m. The total tube length, migrated cells and calcium mineral deposition were quantified in five randomly selected fields. Data represent the mean ± SD of three independent experiments. $^{*}$P<0.05 vs. control group; $^{\#}$P<0.05 vs. PDGF-BB-Ab group. TFRD, total flavonoids of *Rhizoma drynariae*; PDGF, platelet-derived growth factor; ALP, alkaline phosphatase; PA/TA, positive area/total area; EPC, endothelial precursor cell.

and RT-qPCR analyses further verified the role of PDGF-BB in this process, which demonstrated that TFRD significantly upregulated the expression levels of p-PDGF-BB, VEGF, RUNX2 and OSX at the protein and mRNA levels during DO, however, this effect was blocked by PDGF-BB-Ab. It is of note that TFRD also contributed to the increase of p-AKT and p-ERK1/2, which are the primary downstream mediators of the well-known PDGF-BB pathway. Overall, the

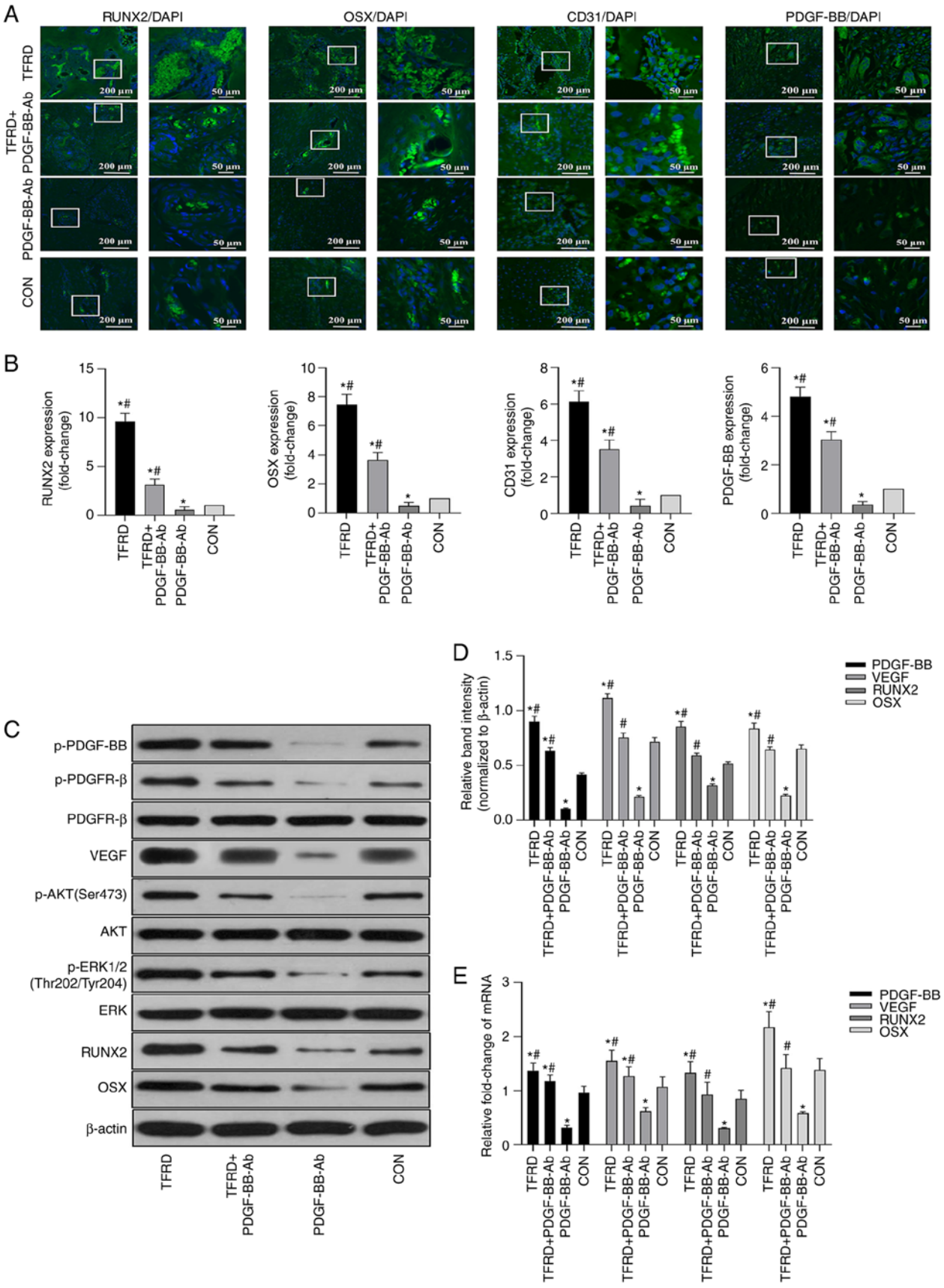


Figure 6. TFRD promotes CD31$^{hi}$Emcn$^{hi}$ vessel formation in angiogenic-osteogenic coupling during distraction osteogenesis via the PDGF-BB/PDGFR-β pathway. (A) Representative immunofluorescence images and (B) quantification of RUNX2, OSX, CD31 and PDGF-BB in the distracted tibias after distraction for 4 weeks. (C) Representative western blotting images and (D) semi-quantitative analyses of PDGF-BB, VEGF, RUNX2, OSX as well as the phosphorylation of AKT and ERK1/2 in the distracted tibias at 4 weeks post-distraction. (E) Quantification of mRNA expression levels of PDGF-BB, VEGF, RUNX2 and OSX. Data represent the mean ± SD. n=3 rats in each group from three independent experiments. $^{*}$P<0.05 vs. control group; $^{\#}$P<0.05 vs. PDGF-BB-Ab group. TFRD, total flavonoids of *Rhizoma drynariae*; PDGF, platelet-derived growth factor; Emcn, endomucin; PDGFR-β, platelet-derived growth factor receptor-β; RUNX2, runt-related transcription factor 2; OSX, Osterix; p-, phosphorylated.

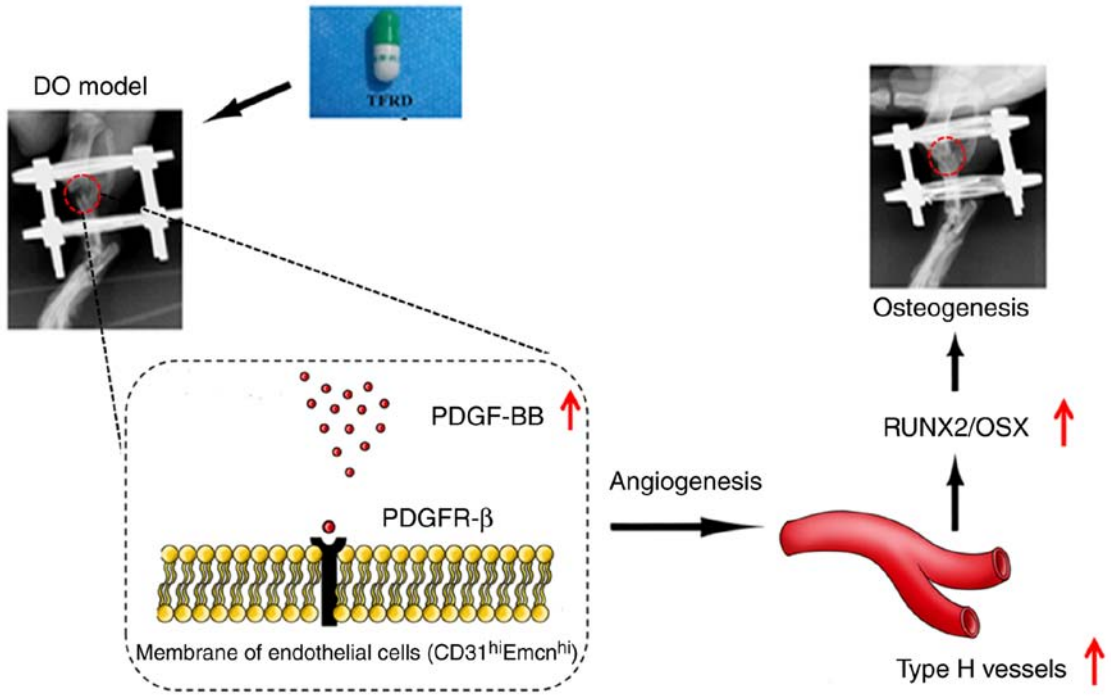


Figure 7. Schematic diagram of the underlying mechanism of TFRD-regulated $CD31^{hi}Emcn^{hi}$ vessel formation and subsequent bone regeneration during DO. TFRD, total flavonoids of *Rhizoma drynariae*; PDGF, platelet-derived growth factor; RUNX2, runt-related transcription factor 2; OSX, Osterix; Emcn, endomucin; PDGFR-β, platelet-derived growth factor receptor-β; DO, distraction osteogenesis.

present results demonstrated that the PDGF-BB/PDGFR-β pathway mediated the formation of $CD31^{hi}Emcn^{hi}$ vessels and TFRD could attenuate the reduction in $CD31^{hi}Emcn^{hi}$ vessel generation caused by blocking PDGF-BB (Fig. 7).

## Discussion

As an endogenous bone tissue engineering technique (34), DO has applications in the regeneration and reconstruction of bone, however it still shows unsatisfactory osteogenesis effects and unclear underlying mechanisms, thus there is an urgent need to address these issues (9). Previous studies have primarily explored mechanical stimulation and bone-related growth factors, thus to the best of our knowledge, the present study is the first to investigate the regulatory functions of $CD31^{hi}Emcn^{hi}$ vessels and the role of angiogenic-osteogenic coupling in DO.

The importance of angiogenesis in bone homeostasis and repair has been established. Bone repair requires new blood vessel formation and endothelial cell-derived molecular signals (35). It is hypothesized that the osteogenesis-promoting effect of the bone vasculature in physiological settings is attributed to $CD31^{hi}Emcn^{hi}$ vessels (17,18) that can enhance angiogenic-osteogenic coupling for bone repair. The abundance of $CD31^{hi}Emcn^{hi}$ vessels has been suggested as a possible sensitive biomarker of bone mass and may represent a potential target for promoting bone repair (36). In the present study, $CD31^{hi}Emcn^{hi}$ vessels were first identified by co-immunofluorescence staining of CD31 and Emcn in the rat DO model, it was also found that TFRD promoted $CD31^{hi}Emcn^{hi}$ vessel generation via the upregulation of PDGF-BB expression, which further enhanced bone and vessel formation during DO. As evidenced by micro-CT, angiographic and histological arrays in the present study, the TFRD-treated group with a high abundance of $CD31^{hi}Emcn^{hi}$ vessels were observed to have increased bone and vessel formation in the distracted gaps, which was further confirmed by the upregulation of RUNX2, OSX, CD31 and PDGF-BB in the immunofluorescent arrays. Furthermore, the *in vitro* ALP and Von Kossa staining assays, as well as the tube formation assay, were performed to verify the pro-osteogenic and angiogenic effects of TFRD on BMSCs and EPCs in the mechanical environment. It was demonstrated that TFRD significantly elevated the osteogenic capacity of BMSCs and the angiogenic capacity of EPCs under stress conditions. By contrast, the PDGF-BB-Ab group, which showed a low abundance of $CD31^{hi}Emcn^{hi}$ vessels, also demonstrated less bone and vessel formation in the distracted gaps, and the osteogenic and angiogenic potentials of BMSCs and EPCs were suppressed in this group,. These results indicated that PDGF-BB mediated the formation of $CD31^{hi}Emcn^{hi}$ vessels, which was consistent with previous studies (20,37).

Of note, although several studies have reported that PDGF-BB secreted by preosteoclasts can induce angiogenic-osteogenic coupling by increasing the abundance of $CD31^{hi}Emcn^{hi}$ vessels in bone (20,37), the underlying mechanism of the induction of $CD31^{hi}Emcn^{hi}$ vessels in the DO model may be different. As reported previously, EPCs, not preosteoclasts, were found to be closely associated with the DO process (7). Aside from influencing the migration and osteogenic differentiation of BMSCs (38), mechanical stimulation could mobilize EPCs from the bone marrow into the peripheral blood and then promote the homing of EPCs to the distracted gaps during the distraction stage and remain in the consolidation stage (39). EPCs that are positive for CD31 and Emcn can differentiate into ECs and further develop into

CD31$^{hi}$Emcn$^{hi}$ vessels, which is of great significance to bone regeneration during DO. In addition, PDGF-BB is proposed to induce the proliferation, migration and angiogenesis of EPCs (40) that further stimulate the activity of BMSCs via PDGF-BB induction (32). Moreover, it is also speculated that PDGF-BB mobilizes cells of mesenchymal origin, stabilizes newly formed vessels and orchestrates cellular components for osteoblast differentiation (41). Therefore, it is hypothesized that the underlying mechanism by which TFRD promotes the formation of CD31$^{hi}$Emcn$^{hi}$ vessels may be via augmenting the activity of PDGF-BB secreted by EPCs rather than preosteoclasts during DO.

As shown in the present study, TFRD administration to the rats significantly increased the abundance of CD31$^{hi}$Emcn$^{hi}$ vessels. However, the effect was notably blocked by PDGF-BB-Ab and blocking PDGF-BB resulted in an obvious decrease of CD31$^{hi}$Emcn$^{hi}$ vessels in the DO model. Moreover, the western blotting and RT-qPCR analyses further demonstrated that exposure of EPCs to PDGF-BB-Ab under stress conditions downregulated the expression levels of p-PDGF-BB, VEGF, RUNX2 and OSX. As commonly known, AKT and p-ERK1/2 are the primary downstream mediators of the well-known PDGF-BB pathway (42) and are involved in angiogenesis and osteogenesis (39,43,44). The present results revealed that the levels of activated AKT and ERK1/2 were significantly increased after TFRD treatment, but significantly reduced by blocking PDGF-BB, which indicated that TFRD may enhance CD31$^{hi}$Emcn$^{hi}$ vessel formation during DO via the PDGF-BB-mediated signaling pathway. To the best of our knowledge, this study is the first to demonstrate that TFRD can enhance angiogenic-osteogenic coupling by promoting PDGF-BB-mediated CD31$^{hi}$Emcn$^{hi}$ vessel generation and subsequent bone repair during DO. In addition, although naringin and neoeriocitrin are the primary active compounds in TFRD, the pharmacological effects of naringin and neoeriocitrin are not completely equivalent to those of TFRD. As reported previously, naringin has been found to exert positive effects on proliferation and osteogenic differentiation of BMSCs and MC3T3-E1 cells, but was found to make little difference to proliferation and angiogenesis of EPCs (25,45,46). By contrast, our previous study indicated that TFRD could promote callus and vessel formation inside the bone defect gap during DO (26). More importantly, it was found in the present study that TFRD could facilitate specific CD31$^{hi}$Emcn$^{hi}$ vessel formation, which is a novel finding concerning the pharmacological effects of TFRD. However, whether this effect is related to naringin, neoeriocitrin or other active ingredients of TFRD remains unclear. At present, the effect of naringin or neoeriocitrin on CD31$^{hi}$Emcn$^{hi}$ vessels has not yet been reported, and little research on this topic has been performed. Therefore, in order to improve our knowledge and investigate all possible pharmacological effects of TFRD, it is necessary to select naringin or neoeriocitrin as a positive control in future studies.

In conclusion, the present study provided the first evidence that TFRD could facilitate CD31$^{hi}$Emcn$^{hi}$ vessel formation and subsequently enhance angiogenic-osteogenic coupling during DO via the PDGF-BB/VEGF/RUNX2/OSX signaling axis. Moreover, CD31$^{hi}$Emcn$^{hi}$ vessels may have potential as a novel therapeutic target for DO, and TFRD may represent a promising drug for promoting bone regeneration in DO. Thus, the present study offered a novel insight into the underlying mechanism of DO-induced bone regeneration.

**Acknowledgements**

Not applicable.

**Funding**

The present study was supported by the National Natural Science Foundations of China (grant no. 81774337), the Basic Research Project of Science and Technology Department of Yunnan Province (grant nos. 202101AZ070001-123, 202201AU070120), the Doctoral Fund Project of Kunming Municipal Hospital of Traditional Chinese Medicine, and Kunming Health Science and Technology Talent Cultivation Project and 'Ten Hundred Thousand' talent project [grant no. 2020-SW (Reserve Personnel)-52].

**Availability of data and materials**

All data generated or analyzed during this study are included in this published article.

**Authors' contributions**

ZS, ZC and GC designed the study and prepared the manuscript. ZS, YZ, HL, HC and MH performed the animal experiments. YZ and ZL performed the cell experiments. ZS and ZC analyzed the data. The research was conceived by WD and ZJ. Data acquisition was performed by WD and YG. ZS and ZJ confirm the authenticity of all the raw data. The custom-made circle external device was designed by ZJ. All authors have read and approved the final manuscript.

**Ethics approval and consent to participate**

All animal care and experimental procedures were approved by the Institutional Animal Ethics Committee of the First Affiliated Hospital of Guangzhou University of Traditional Chinese Medicine (approval no. TCMF1-2018002; Guangzhou, China).

**Patient consent for publication**

Not applicable.

**Competing interests**

The authors declare that they have no competing interests.

**References**

1. Nauth A, McKee MD, Einhorn TA, Watson JT, Li R and Schemitsch EH: Managing bone defects. J Orthop Trauma 25: 462-466, 2011.
2. Mauffrey C, Barlow BT and Smith W: Management of segmental bone defects. J Am Acad Orthop Surg 23: 143-153, 2015.
3. Li W, Zhu S and Hu J: Bone regeneration is promoted by orally administered bovine lactoferrin in a rabbit tibial distraction osteogenesis model. Clin Orthop Relat Res 473: 2383-2393, 2015.

4. Sun Y, Xu J, Xu L, Zhang J, Chan K, Pan X and Li G: MiR-503 promotes bone formation in distraction osteogenesis through suppressing smurf1 expression. Sci Rep 7: 409, 2017.
5. Sun YX, Zhang JF, Xu J, Xu LL, Wu TY, Wang B, Pan XH and Li G: MiRNA-144-3p inhibits bone formation in distraction osteogenesis through targeting Connexin 43. Oncotarget 8: 89913-89922, 2017.
6. Jia Y, Qiu S, Xu J, Kang Q and Chai Y: Exosomes secreted by young mesenchymal stem cells promote new bone formation during distraction osteogenesis in older rats. Calcif Tissue Int 106: 509-517, 2020.
7. Jia YC, Zhu Y, Qiu S, Xu J and Chai Y: Exosomes secreted by endothelial progenitor cells accelerate bone regeneration during distraction osteogenesis by stimulating angiogenesis. Stem Cell Res Ther 10: 12, 2019.
8. Montes-Medina L, Hernández-Fernández A, Gutiérrez-Rivera A, Ripalda-Cemboráin P, Bitarte N, Pérez-López V, Granero-Moltó F, Prosper F and Izeta A: Effect of bone marrow stromal cells in combination with biomaterials in early phases of distraction osteogenesis: An experimental study in a rabbit femur model. Injury 49: 1979-1986, 2018.
9. Paley D: Problems, obstacles, and complications of limb lengthening by the Ilizarov technique. Clin Orthop Relat Res 250: 81-104, 1990.
10. Dhaliwal R, Kunchur K and Farhadieh R: Review of the cellular and biological principles of distraction osteogenesis: An in vivo bioreactor tissue engineering model. J Plast Reconstr Aesthet Surg 69: e19-e26, 2016.
11. Tomlinson RE and Silva MJ: Skeletal blood flow in bone repair and maintenance. Bone Res 1: 311-322, 2013.
12. Gerber HP and Ferrara N: Angiogenesis and bone growth. Trends Cardiovasc Med 10: 223-228, 2000.
13. Saran U, Piperni SG and Chatterjee S: Role of angiogenesis in bone repair. Arch Biochem Biophys 561: 109-117, 2014.
14. Brandi ML and Collin-Osdoby P: Vascular biology and the skeleton. J Bone Miner Res 21: 183-192, 2006.
15. Grosso A, Burger MG, Lunger A, Schaefer DJ, Banfi A and Maggio ND: It takes two to tango: Coupling of angiogenesis and osteogenesis for bone regeneration. Front Bioeng Biotechnol 5: 68, 2017.
16. Fang TD, Salim A, Xia W, Nacamuli RP, Guccione S, Song HM, Carano RA, Filvaroff EH, Bednarski MD, Giaccia AJ and Longaker MT: Angiogenesis is required for successful bone induction during distraction osteogenesis. J Bone Miner Res 20: 1114-1124, 2005.
17. Kusumbe AP, Ramasamy SK and Adams RH: Coupling of angiogenesis and osteogenesis by a specific vessel subtype in bone. Nature 507: 323-328, 2014.
18. Ramasamy SK, Kusumbe AP, Wang L and Adams RH: Endothelial notch activity promotes angiogenesis and osteogenesis in bone. Nature 507: 376-380, 2014.
19. Peng Y, Wu S, Li Y and Crane JL: Type H blood vessels in bone modeling and remodeling. Theranostics 10: 426-436, 2020.
20. Huang J, Yin H, Rao SS, Xie PL, Cao X, Rao T, Liu SY, Wang ZX, Cao J, Hu Y, *et al*: Harmine enhances type H vessel formation and prevents bone loss in ovariectomized mice. Theranostics 8: 2435-2446, 2018.
21. Xu R, Yallowitz A, Qin A, Wu Z, Shin DY, Kim JM, Debnath S, Ji G, Bostrom MP, Yang X, *et al*: Targeting skeletal endothelium to ameliorate bone loss. Nat Med 24: 823-833, 2018.
22. Wang J, Gao Y, Cheng P, Li D, Jiang H, Ji C, Zhang S, Shen C, Li J, Song Y, *et al*: CD31$^{hi}$Emcn$^{hi}$ Vessels support new trabecular bone formation at the frontier growth area in the bone defect repair process. Sci Rep 7: 4990, 2017.
23. Fan YG and Zhan HS: Orthopaedics of traditional chinese medicine. People's Medical Publishing House, Beijing: 29-31, 2005.
24. Yao W, Zhang H, Jiang X, Mehmood K, Iqbal M, Li A, Zhang J, Wang Y, Waqas M, Shen Y and Li J: Effect of total flavonoids of on tibial dyschondroplasia by regulating BMP-2 and Runx2 expression in chickens. Front Pharmacol 9: 1251, 2018.
25. Chen LL, Lei LH, Ding PH, Tang Q and Wu YM: Osteogenic effect of Drynariae rhizoma extracts and Naringin on MC3T3-E1 cells and an induced rat alveolar bone resorption model. Arch Oral Biol 56: 1655-1662, 2011.
26. Song S, Gao Z, Lei X, Niu Y, Zhang Y, Li C, Lu Y, Wang Z and Shang P: Total flavonoids of drynariae rhizoma prevent bone loss induced by hindlimb unloading in rats. Molecules 22: 1033, 2017.
27. Shen Z, Jiang ZW, Li D, Zhang Y, Li ZG, Chen HM, *et al*: Comparison of two types of tonifying kidney in the mechanism of angiogenesis and osteogenesis coupling based on distraction osteogenesis. Chin J Tradit Chin Med Pharm 34: 2150-2155, 2019.
28. Shen Z, Lin H, Chen G, Zhang Y, Li Z, Li D, Xie L, Li Y, Huang F and Jiang Z: Comparison between the induced membrane technique and distraction osteogenesis in treating segmental bone defects: An experimental study in a rat model. PLoS One 14: e0226839, 2019.
29. Song SH, Zhai YK, Li CQ, Yu Q, Lu Y, Zhang Y, Hua WP, Wang ZZ and Shang P: Effects of total flavonoids from Drynariae Rhizoma prevent bone loss in vivo and in vitro. Bone Rep 5: 262-273, 2016.
30. Yan Y, Chen H, Zhang H, Guo C, Yang K, Chen K, Cheng R, Qian N, Sandler N, Zhang YS, *et al*: Vascularized 3D printed scaffolds for promoting bone regeneration. Biomaterials 190-191: 97-110, 2019.
31. Livak KJ and Schmittgen TD: Analysis of relative gene expression data using real-time quantitative PCR and the 2(-Delta Delta C(T)) method. Methods 25: 402-408, 2001.
32. Zhang M, Ahn W, Kim S, Hong HS, Quan C and Son Y: Endothelial precursor cells stimulate pericyte-like coverage of bone marrow-derived mesenchymal stem cells through platelet-derived growth factor-BB induction, which is enhanced by substance P. Microcirculation 24: e12394, 2017.
33. Naruse K, Yamada T, Sai XR, Hamaguchi M and Sokabe M: Pp125FAK is required for stretch dependent morphological response of endothelial cells. Oncogene 17: 455-463, 1998.
34. Ilizarov GA: The tension-stress effect on the genesis and growth of tissues. Part I. The influence of stability of fixation and soft-tissue preservation. Clin Orthop Relat Res 238: 249-281, 1989.
35. Stegen S, van Gastel N and Carmeliet G: Bringing new life to damaged bone: The importance of angiogenesis in bone repair and regeneration. Bone 70: 19-27, 2015.
36. Wang L, Zhou F, Zhang P, Wang H, Qu Z, Jia P, Yao Z, Shen G, Li G, Zhao G, *et al*: Human type H vessels are a sensitive biomarker of bone mass. Cell Death Dis 8: e2760, 2017.
37. Xie H, Cui Z, Wang L, Xia Z, Hu Y, Xian L, Li C, Xie L, Crane J, Wan M, *et al*: PDGF-BB secreted by preosteoclasts induces angiogenesis during coupling with osteogenesis. Nat Med 20: 1270-1278, 2014.
38. Liu L, Zong C, Li B, Shen D, Tang Z, Chen J, Zheng Q, Tong X, Gao C and Wang J: The interaction between β1 integrins and ERK1/2 in osteogenic differentiation of human mesenchymal stem cells under fluid shear stress modelled by a perfusion system. J Tissue Eng Regen Med 8: 85-96, 2014.
39. Lee DY, Cho TJ, Kim JA, Lee HR, Yoo WJ, Chung CY and Choi IH: Mobilization of endothelial progenitor cells in fracture healing and distraction osteogenesis. Bone 42: 932-941, 2008.
40. Wang H, Yin Y, Li W, Zhao X, Yu Y, Zhu J, Qin Z, Wang Q, Wang K, Lu W, *et al*: Over-expression of PDGFR-β promotes PDGF-induced proliferation, migration, and angiogenesis of EPCs through PI3K/Akt signaling pathway. PLoS One 7: e30503, 2012.
41. Caplan AI and Correa D: PDGF in bone formation and regeneration: New insights into a novel mechanism involving MSCs. J Orthop Res 29: 1795-1803, 2011.
42. Heldin CH, Lennartsson J and Westermark B: Involvement of platelet-derived growth factor ligands and receptors in tumorigenesis. J Intern Med 283: 16-44, 2018.
43. Lee SJ, Namkoong S, Kim YM, Kim CK, Lee H, Ha KS, Chung HT, Kwon YG and Kim YM: Fractalkine stimulates angiogenesis by activating the Raf-1/MEK/ERK-and PI3K/Akt/eNOS-dependent signal pathways. Am J Physiol Heart Circ Physiol 291: H2836-H2846, 2006.
44. Zhang J, Guan J, Qi X, Ding H, Yuan H, Xie Z, Chen C, Li X, Zhang C and Huang Y: Dimethyloxaloxaloylglycine promotes the angiogenic activity of mesenchymal stem cells derived from iPSCs via activation of the PI3K/Akt pathway for bone regeneration. Int J Biol Sci 12: 639-652, 2016.
45. Kuang MJ, Zhang WH, He WW, Sun L, Ma JX, Wang D and Ma XL: Naringin regulates bone metabolism in glucocorticoid-induced osteonecrosis of the femoral head via the Akt/Bad signal cascades. Chem Biol Interact 304: 97-105, 2019.
46. Zhang P, Dai KR, Yan SG, Yan WQ, Zhang C, Chen DQ, Xu B and Xu ZW: Effects of naringin on the proliferation and osteogenic differentiation of human bone mesenchymal stem cell. Eur J Pharmacol 607: 1-5, 2009.